

Percentile-specific computational phantoms constructed from ICRP mesh-type reference computational phantoms (MRCPs)

Hanjin Lee¹, Yeon Soo Yeom², Thang Tat Nguyen³, Chansoo Choi¹, Haegin Han¹, Bangho Shin¹, Xujia Zhang¹, Chan Hyeong Kim^{1,6}, Beom Sun Chung⁴ and Maria Zankl⁵

¹ Department of Nuclear Engineering, Hanyang University, 222 Wangsimni-ro, Seongdong-gu, Seoul, 04763, Republic of Korea

² Division of Cancer Epidemiology & Genetics, National Cancer Institute, 9609 Medical Center Drive, Bethesda, MD 20892-9760, USA

³ School of Nuclear Engineering and Environmental Physics, Hanoi University of Science and Technology, 1 Dai Co Viet road, Hai Ba Trung district, Hanoi, Vietnam

⁴ Department of Anatomy, Ajou University School of Medicine, 164 Worldcup-ro, Suwon, Gyeonggi-do, 16499, Korea

⁵ Helmholtz Zentrum München German Research Center for Environmental Health, Institute of Radiation Protection, Ingolstädter Landstraße 1, 85764 Neuherberg, Germany

⁶ Author to whom any correspondence should be addressed

E-mail: chkim@hanyang.ac.kr

Abstract

Recently, the Task Group 103 of the International Commission on Radiological Protection (ICRP) has developed new mesh-type reference computational phantoms (MRCPs) for adult male and female. When compared to the current voxel-type reference computational phantoms in ICRP Publication 110, the MRCPs have several advantages, including deformability which makes it possible to create phantoms in different body sizes or postures. In the present study, the MRCPs were deformed to produce a set of percentile-specific phantoms representing the 10th, 50th, and 90th percentiles of standing height and body weight in Caucasian population. For this, anthropometric parameters for the percentile-specific phantoms were first derived from the anthropometric software and survey data. Then, the MRCPs were modified to match the derived anthropometric parameters. For this, first, the MRCPs were scaled in the axial direction to match the head height, torso length, and leg length. Then, the head, torso, and legs were scaled in the transversal directions to match the lean body mass for the percentile-specific phantoms. Finally, the scaled phantoms were manually adjusted to match the body weight and the remaining anthropometric parameters (upper arm, waist, buttock, thigh, and calf circumferences and sagittal abdominal diameter). The constructed percentile-specific phantoms and the MRCPs were implemented into the Geant4 Monte Carlo code to calculate organ doses for a cesium-137 contaminated floor. The results showed that organ doses of the 50th percentile (both standing height and body weight) phantoms are very close to those of the MRCPs. There were noticeable differences in organ doses, however, for the 10th and 90th percentile phantoms when compared with those of the MRCPs. The results of the present study confirm the general intuition that a small person receives higher doses than a large person when exposed to a static radiation field, and organs closer to the source receive higher doses.

Keywords: mesh-type reference computational phantom, non-reference phantom, percentile-specific phantom, body size, Monte Carlo

1. Introduction

To perform an individualized dosimetry for retrospective dose reconstruction (Clairand *et al* 2008, Courageot *et al* 2010, Lu *et al* 2017) or virtual calibration of counters (Pierrat *et al* 2005, Bochud *et al* 2014, Chen *et al* 2016) based on Monte Carlo modeling, it would be ideal to use a computational human phantom which is directly produced using a tomographic image (i.e., from computed

tomography (CT) or magnetic resonance imaging (MRI)) of the individual of interest. For most cases, however, it is neither practical nor necessary to directly produce a computational phantom for the individual considering that it will require not only a CT or MRI imaging for the individual, but also time-consuming phantom construction. Therefore, it is considered as a practical solution to modify existing computational phantoms to create phantoms with various body sizes in advance and to use one of the phantoms which best fits the individual (Geyer *et al* 2014, Akhavanallaf *et al* 2018).

Several research groups (Johnson *et al* 2009, Na *et al* 2010, Cassola *et al* 2011, Ding *et al* 2012, Geyer *et al* 2014) have modified their own existing phantoms to construct different-size or percentile-specific phantoms. For example, Cassola *et al* (2011) modified the MASH3 and FASH3 phantoms to construct 18 phantoms which represent 10th, 50th, and 90th percentile standing height and body weight in male and female Caucasian populations. Na *et al* (2010) modified the RPI-AM and RPI-AF phantoms to construct percentile-specific phantoms. The RPI-AM and RPI-AF phantoms were also modified to construct a set of obese phantoms with 5 different body weights with the same standing height for each gender considering both subcutaneous and visceral adipose tissue growth (Ding *et al* 2012). Johnson *et al* (2009) developed a methodology to construct percentile-specific phantoms for the UF/NCI family of hybrid phantoms and constructed 25 different adult male and 15 pediatric female phantoms for U.S. population for the purpose of demonstrating the methodology. Extending the work of Johnson *et al* (2009), Geyer *et al* (2014) established a phantom library, containing 193 adult and 158 pediatric phantoms, to cover the body sizes of the entire U.S. population.

Recently, the International Commission on Radiological Protection (ICRP) Task Group 103 developed new adult male and female mesh-type reference computational phantoms (MRCPs) (Kim *et al* 2018). The MRCPs were constructed by converting the current voxel-type reference computational phantoms (VRCPs) of ICRP Publication 110 (ICRP 2009) into a high-quality/fidelity mesh format, addressing the limitations of the VRCPs due to their limited voxel resolutions and the nature of voxel geometry. The MRCPs include all the source and target organs/tissues required for effective dose calculation, including the micron-scale regions such as the stem cell layers in the alimentary and respiratory tract organs which were not modelled in the VRCPs. Note that the MRCPs can be directly used in Monte Carlo codes for dose calculation where the advantages of mesh geometry are fully maintained, while a so-called ‘voxelization’ process is required for most existing mesh phantoms (Kim *et al* 2011, Yeom *et al* 2014). In addition, the mesh geometry of the MRCPs provides deformability, which encouraged us to deform the phantoms to non-reference-size phantoms with different body sizes to be used for individualized dosimetry.

In the presented study, we modified the MRCPs to develop a total of 18 percentile-specific adult male and female phantoms that represent 10th, 50th, and 90th percentile standing heights and body weights in male and female Caucasian populations. Prior to the modification, the standing height, body weight, and additional 10 anthropometric parameters were derived from the data extracted from the *PeopleSize 2008 Professional* software, the National Health and Nutrition Examination Survey (NHANES) database, and the US Army Anthropometric Survey (ANSUR II) database. The MRCPs were then scaled in the axial direction (i.e., z direction) of the body to match the derived values of head height, torso length, and leg length and in the transverse directions (i.e., x and y directions) to match the lean body mass (LBM) for the given standing height and body weight of the percentile-specific phantoms. The scaled phantoms were finally adjusted to match the body weight and the remaining anthropometric parameters (upper arm, waist, buttock, thigh, and calf circumferences and sagittal abdominal diameter). After the construction of the phantoms, the effect and validity of scaling

and adjustments were investigated by calculating organ depth and cord length distributions and by comparing the organ masses with some available autopsy data. The constructed phantoms and the MRCPs were then implemented into the Geant4 Monte Carlo code to calculate organ doses for a cesium-137 contaminated floor, and the calculated values were compared to see the dosimetric influence of the differences in body sizes.

2. Materials and Method

2.1 The mesh-type reference computational phantoms (MRCPs)

Figure 1 shows the adult male and female mesh-type reference computational phantoms (MRCPs) developed by the ICRP Task Group 103 (Kim *et al* 2018). The standing height and body weight of the MRCPs are consistent with the reference values of ICRP Publication 89 (2002) (i.e., male: 176 cm and 73 kg; female: 163 cm and 60 kg). The MRCPs contain 48 organs/tissues with 170 regions including those needed to calculate effective dose. The phantoms also include tens-of-micron-thick source and target regions in the eye lens, skin, urinary bladder, alimentary tract organs, and respiratory tract organs. The organ/tissue masses of the MRCPs are consistent with the reference values in ICRP Publications 89 (2002), inclusive of blood content, within 0.1% of deviation.



Figure 1. MRCPs for adult male (left) and female (right).

2.2 Derivation of anthropometric parameters

2.2.1 Standing height and body weight

In the present study, the adult MRCPs were modified to produce a set of percentile-specific phantoms which represent 10th, 50th, and 90th percentile standing heights and body weights of adult male and female Caucasian populations. For this, first, the 10th, 50th, and 90th percentile standing heights of male and female were extracted for each of the nine countries (i.e., Sweden, Netherlands, Germany, Belgium, Australia, USA, France, UK, and Italy), following the approach used by Cassola *et al* (2011), from the *PeopleSize 2008 Professional* software (www.openenerg.com), as shown in table 1. In the extracted data for each country, we selected the age group which is closest to the age range of adults (= 20 to 50 years) considered in the ICRP Publication 89 (2002) (see table 1). Then, for each of the 10th, 50th, and 90th percentile standing heights, the 10th, 50th, and 90th percentile body weights were extracted, as shown in table 2. The extracted values of standing height and body weight were finally averaged for the nine countries, reflecting the population estimates of the 20–49 age group in 2015 provided in the UN World Population Prospects 2017 revision (UN-DESA 2017), to obtain the values of the 10th, 50th, and 90th percentile standing heights and body weights for the entire Caucasian population.

Table 1. 10th, 50th, and 90th standing heights in male and female Caucasian populations.

(unit: centimeters)

| Country | Age group (years) | Standing height percentile | | | | | |
|-------------|-------------------|----------------------------|------------------|------------------|------------------|------------------|------------------|
| | | Male | | | Female | | |
| | | 10 th | 50 th | 90 th | 10 th | 50 th | 90 th |
| Sweden | 18-65 | 169.5 | 178.6 | 187.6 | 158.7 | 167.6 | 176.4 |
| Netherlands | 18-64 | 169.9 | 179.2 | 188.6 | 158.2 | 166.1 | 173.9 |
| Germany | 20-50 | 168.7 | 177.8 | 186.8 | 157.7 | 166.2 | 174.7 |
| Belgium | 18-65 | 166.9 | 176.6 | 186.3 | 155.9 | 164.6 | 173.3 |
| Australia | 25-50 | 167.9 | 176.7 | 185.5 | 155.7 | 163.9 | 172.0 |
| USA | 25-50 | 167.3 | 177.0 | 186.6 | 154.6 | 163.1 | 171.6 |
| France | 18-70 | 166.7 | 175.6 | 184.5 | 154.2 | 162.5 | 170.8 |
| UK | 25-50 | 167.5 | 176.4 | 185.4 | 154.3 | 162.7 | 171.0 |
| Italy | 18-83 | 163.2 | 172.1 | 181.0 | 151.6 | 159.8 | 167.9 |

Table 2. 10th, 50th, and 90th body weights for people who have 10th, 50th, and 90th standing heights in Caucasian populations.

(unit: kilograms)

| Country | Standing height percentile | Body weight percentile | | | | | |
|-------------|----------------------------|------------------------|------------------|------------------|------------------|------------------|------------------|
| | | Male | | | Female | | |
| | | 10 th | 50 th | 90 th | 10 th | 50 th | 90 th |
| Sweden | 10 th | 56 | 63 | 71 | 50 | 54 | 57 |
| | 50 th | 68 | 75 | 83 | 58 | 61 | 64 |
| | 90 th | 84 | 91 | 99 | 71 | 74 | 78 |
| Netherlands | 10 th | 60 | 67 | 73 | 52 | 56 | 59 |
| | 50 th | 71 | 77 | 84 | 61 | 65 | 69 |
| | 90 th | 85 | 91 | 98 | 77 | 81 | 85 |
| Germany | 10 th | 58 | 66 | 75 | 44 | 49 | 55 |
| | 50 th | 71 | 79 | 88 | 57 | 63 | 68 |
| | 90 th | 89 | 97 | 105 | 80 | 85 | 90 |
| Belgium | 10 th | 56 | 64 | 71 | 49 | 54 | 58 |
| | 50 th | 68 | 76 | 83 | 60 | 65 | 69 |
| | 90 th | 84 | 92 | 99 | 79 | 83 | 88 |
| Australia | 10 th | 62 | 70 | 78 | 46 | 51 | 57 |
| | 50 th | 75 | 83 | 91 | 59 | 65 | 70 |
| | 90 th | 92 | 100 | 108 | 82 | 88 | 93 |
| USA | 10 th | 55 | 65 | 76 | 43 | 50 | 57 |
| | 50 th | 72 | 82 | 93 | 60 | 67 | 74 |
| | 90 th | 95 | 105 | 116 | 90 | 97 | 104 |
| France | 10 th | 55 | 62 | 69 | 44 | 48 | 52 |
| | 50 th | 66 | 73 | 80 | 54 | 58 | 62 |
| | 90 th | 81 | 88 | 95 | 70 | 74 | 78 |
| UK | 10 th | 59 | 67 | 75 | 45 | 51 | 56 |
| | 50 th | 72 | 80 | 88 | 58 | 64 | 69 |
| | 90 th | 89 | 98 | 106 | 81 | 87 | 92 |
| Italy | 10 th | 52 | 59 | 67 | 45 | 48 | 51 |
| | 50 th | 64 | 71 | 78 | 53 | 56 | 59 |
| | 90 th | 79 | 87 | 94 | 65 | 68 | 71 |

2.2.2 Secondary anthropometric parameters

A total of ten additional anthropometric parameters (i.e., sitting height; head height, length, and breadth; sagittal abdominal diameter; and upper arm, waist, buttock, thigh, and calf circumferences) were derived to produce percentile-specific phantoms. Again, the *PeopleSize* software was used to derive the values of sitting height and head height for the percentile-specific phantoms assuming that these parameters depend only on standing height.

The value of sitting height, which is the 50th percentile value for the people with a given standing height percentile, was directly extracted from the *PeopleSize* software.

The head dimensions (i.e., height, length, and breadth) of the MRCPs were found to be significantly different from those derived from anthropometric data. For the head, therefore, we used a different approach. That is, in the present study, the head of the percentile-specific phantom was not directly matched to the head dimensions derived from anthropometric data, but adjusted for the same degree of change in head dimensions. For this adjustment, the head heights (i.e., from chin to top of head) were first determined for the standing heights of the percentile-specific phantom and the MRCP by linear regression of the head height data for the five countries (i.e., Germany, Belgium, Australia, USA, and UK) available in the *PeopleSize* software. Then, the head height for the percentile-specific phantom was calculated by multiplying the head height of the MRCP with the ratio of the head heights determined for the standing heights of the percentile-specific phantom and the MRCP. A similar approach was used to derive the values of head breadth and length for the percentile-specific phantom. The organs of the head were assumed to vary with the changes of the head dimensions. The main advantage of this ratio approach is that we can minimize the degree of scaling for the eyes, which are among the organs considered important in radiation protection; the change in the volume of the eye model was at most 11% and 13% for the male and female phantom, respectively.

The other anthropometric parameters depend not only on standing height but also on body weight, but the *PeopleSize* software does not provide anthropometric parameters as a function of multiple parameters; therefore, these anthropometric parameters were derived from other databases. The target values of upper arm, waist, buttock, thigh, and calf circumferences and sagittal abdominal diameter were derived from the data extracted from the National Health and Nutrition Examination Survey (NHANES) database which is a survey research program conducted by the National Center for Health Statistics of the Centers for Diseases (www.cdc.gov/nchs/nhanes.html). Specifically, the data of the Continuous NHANES (1999–2014) database was used for sagittal abdominal diameter and upper arm, thigh, waist, and calf circumferences, and the data of the NHANES III (1988–1994) database was used for buttock circumference due to the absence of the data in the updated Continuous NHANES database. Head length and breadth, absent from the NHANES, were derived from the US Army Anthropometric Survey (ANSUR II) database which is the database of US Army subjects recently established by the Natick Soldier Research, Development and Engineering Center in 2012 (Gordon *et al* 2014). The values of these anthropometric parameters for the percentile-specific phantoms were derived from multiple linear regression of the data as a function of standing height and body weight.

2.3 Phantom construction

2.3.1 Scaling

In the present study, the values of the anthropometric parameters derived above serve as the target values to which the MRCPs are adjusted to produce percentile-specific phantoms. The percentile-specific phantoms were mainly constructed by scaling in the axial (i.e., z direction) and transversal directions (i.e., x and y directions), followed by manual adjustments for the skin (= exterior surface) and breasts to match the body weight and the remaining anthropometric parameters to the target values. For scaling, an MRCP was divided into three parts: head, torso (including arms), and legs. Then, each part was scaled separately. First, the head was scaled in the axial direction with the ratio method explained earlier. Then, the torso was scaled in the axial direction to match the sitting height (= torso length + head height) of the phantom to the target value of sitting height. Finally, the legs were scaled in the axial direction to match the target values of leg length.

After scaling in the axial direction, the MRCP was scaled in the transverse directions. In the present study, the torso and legs were scaled using different scaling factors derived to match the lean body mass (LBM). Note that the LBM is the body weight devoid of the body fat, which is strongly correlated not only to internal organ/tissue mass (Bosy-Westphal 2004), but also to standing height and body weight (Hume 1966, James and Waterlow 1976, Boer 1984, Deurenberg *et al* 1991, Pieterman *et al* 2002). In the present study, the following equation (Deurenberg *et al* 1991, Pieterman *et al* 2002) was used to calculate the LBM for a given standing height and body weight of a percentile-specific phantom:

$$LBM = W - \left[W \times \frac{1.2 \times \left(\frac{W}{H^2} \right) + 0.23 \times A - G}{100} \right] \quad (1)$$

where LBM is the lean body mass (kg), W is the body weight (kg), H is the standing height (cm), A is the age (years), and G is a gender-dependent parameter of 16.2 for male and 5.4 for female. This equation was derived based on the body fat data measured for 1229 subjects (male: 521 and female: 708) with a wide range in the age (7–83 years) and the body mass index (BMI: 13.9–40.9 kg/m²) (Deurenberg *et al* 1991). Note that the LBM estimated with the equation using the standing height and body weight of the MRCP shows a good agreement with the LBM of the MRCP, for both the male and female phantom, the difference being only 0.16% and 0.36% for the male and female phantom, respectively. For the estimation, in the present study, the age (A) was assumed to be 35 years, the average value of the age range of adults considered in the ICRP Publication 89 (2002). In order to match the LBM in consideration of the torso or leg length, scaling factors in the transverse directions were derived for each part, following the approach used by Qiu *et al* (2008). The torso including the arms was scaled in the transversal directions using a scaling factor calculated by the LBMs as follows:

$$SF_{x,y}^{torso} = \left(\frac{LBM_{target} / LBM_{MRCP}}{R_z^{torso}} \right)^{0.5} \quad (2)$$

where $SF_{x,y}^{torso}$ is the scaling factor for the torso in the transversal directions, R_z^{torso} is the ratio of the target torso length and the MRCP torso length, LBM_{target} is the LBM estimated for the target percentile-specific phantom, and LBM_{MRCP} is the LBM of the MRCP.

Likewise, a scaling factor of the legs in the transversal directions was calculated by the following equation:

$$SF_{x,y}^{legs} = \left(\frac{LBM_{target} / LBM_{MRCP}}{R_z^{legs}} \right)^{0.5} \quad (3)$$

where $SF_{x,y}^{legs}$ is the scaling factor for the legs in the transversal directions, R_z^{legs} is the ratio of the target leg length and the MRCP leg length.

For the scaling of the head in the transversal directions, the ratio approach was used which was previously used to scale the head in the axial direction. The head breadths (the maximum horizontal breadth of the head above the ears) were first determined for the target standing height and body weight and the MRCP standing height and body weight by multiple linear regression of the head height data as a function of standing height and body weight. Then, the target head breadth was calculated by multiplying the MRCP head breadth by the ratio of the head breadths of the target standing height and body weight and the MRCP standing height and body weight. This approach was also used to derive the target value of head length (i.e., the distance from the glabella landmark between the brow ridges to opisthocranion).

The scaling approach using the scaling factors derived above, however, resulted in slight dislocations at the boundaries of the body parts (head, torso, and legs) due to the differences in the transversal scaling factors for the head, torso, and legs. In the present study, therefore, the transversal scaling factors were modified to linearly change in the axial direction. That is, the scaling factor for the legs was modified to linearly change in the axial direction from the scaling factor of the torso (at the top of the legs) to the scaling factor of the legs (at the middle of the legs). For the head, the transversal scaling factor was modified to change linearly, from the scaling factor of the torso (at the bottom of the head) to the scaling factor of the head (at each measurement level of the head dimension), then from the scaling factor of the head (at each measurement level of the head dimension) to unity (at the top of the head).

2.3.2 Adjustment for skin and breasts

After the scaling of the phantom, the skin and breasts were adjusted manually as follows. For the skin, assuming that the skin mass is proportional to the body surface area, the target mass of the skin was determined using the following equation:

$$SM_{target}(\text{kg}) = SM_{MRCP}(\text{kg}) \times BSA_{target}(m^2) / BSA_{MRCP}(m^2) \quad (4)$$

where SM_{target} and BSA_{target} are the skin mass and body surface area of the target percentile-specific phantom, respectively, and SM_{MRCP} and BSA_{MRCP} are the skin mass and body surface area of the MRCP. The BSA_{target} was calculated by using the following equation given in ICRP Publication 89 (2002):

$$BSA(m^2) = 0.0235 \times H^{0.42246} \times W^{0.51456} \quad (5)$$

where H is the standing height (cm) and W is the body weight (kg). Considering both the target skin

mass and the target values of the remaining anthropometric parameters (i.e., upper arm, waist, buttock, thigh, and calf circumferences and sagittal abdominal diameter), the exterior skin surface was manually adjusted using the *Deform* function of the *Rapidform* software (INUS Technology Inc., Korea). Note that the deformed exterior skin surfaces of the phantoms were confirmed by a group of anatomists. Then, the deformed exterior skin surface was replicated to produce three additional surfaces. Then, one of the surfaces was reduced in size, by using the offset function of the software, to redefine the inner skin surface, exactly matching the target skin mass. The other two surfaces were also reduced to redefine the radiosensitive target layer in the skin at a depth of 50-100 μm from the exterior skin surface.

The breasts were finally adjusted assuming that the change in the mass of breast adipose tissue is directly proportional to that of the residual soft tissue (RST) which is mainly composed of adipose tissue. That is, the breasts of the scaled phantom were adjusted to preserve the ratio of the masses of the breast adipose tissue to RST of the MRCP. In addition, following a recommendation of the anatomists, the breasts were slightly repositioned to preserve the ratio of the breast-center-to-skin and breast-center-to-muscle distances (in the anteroposterior direction) of the MRCP.

2.4 Monte Carlo dose calculations

The 10th, 50th, and 90th percentile phantoms (i.e., M_H10W10, M_H50W50, M_H90W90, F_H10W10, F_H50W50, and F_H90W90) which represent small, average, and large people, respectively, and the MRCPs were implemented in the Geant4 Monte Carlo code (ver. 10.03) (Allison *et al* 2016) to calculate the organ doses (= organ/tissue averaged absorbed doses) for the radiation exposure scenario described in Eakins (2015), in which cesium-137 is uniformly distributed on the surface of the floor (see figure 2). In this simulation, cesium-137 gammas were isotropically emitted on a disk of radius 200 cm below the feet of the phantom, using the *G4GeneralParticleSource*, and the phantom was assumed to be in air.

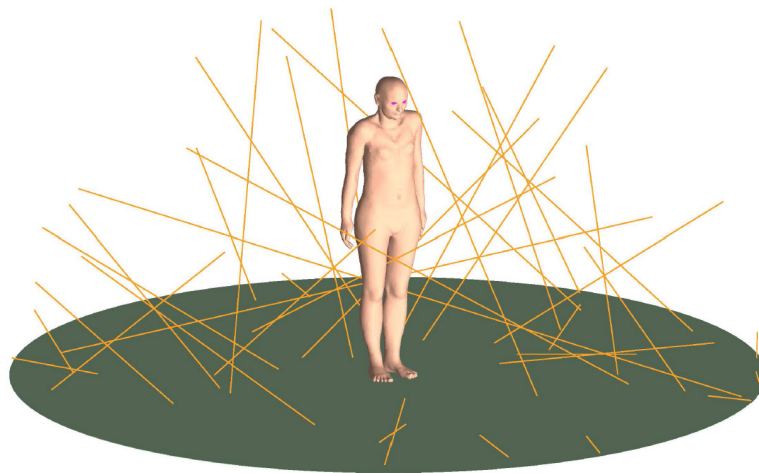


Figure 2. Monte Carlo simulation geometry for cesium-137 contamination on floor. Phantom is irradiated by photons isotropically emitted on disk of 200 cm radius below feet of phantom.

For implementation, the constructed percentile-specific phantoms in the polygonal-mesh format were first converted into tetrahedral-mesh format using the TetGen code (Si 2006), and then these phantoms were implemented in the Geant4 code by using the *G4Tet* class, following the method used

in Yeom *et al* (2014). To transport photons and electrons, the electromagnetic physics library of *G4EmLivermorePhysics* was used with the secondary production cut value of 1 mm. The organ doses were calculated to have a relative error of less than 1% by transporting sufficient number of particles ($= 4.2 \times 10^9$ particles). Variation reduction techniques (VRTs) were not used. Most organ/tissue doses were directly calculated using the *G4PSEnergyDeposit* class, but absorbed doses to the skeletal tissues (i.e., red bone marrow (RBM) and bone surface) were estimated by using the fluence-to-absorbed dose response functions (DRFs) in ICRP Publication 116 (2010).

3. Results and Discussion

3.1. Percentile-specific anthropometric parameters

Table 3 shows the values of the 10th, 50th, and 90th percentile standing heights and body weights derived in the present study for adult male and female to which the MRCPs were matched to produce percentile-specific phantoms. For standing height, it can be seen that the difference between 10th and 50th percentiles is close to the difference between 50th and 90th percentiles. For body weight, on the other hand, it can be seen that the difference between 10th and 50th percentiles is much smaller than the difference between 50th and 90th percentiles. This is mainly because the biologic lower limit of the body weight exists; that is, the body weight cannot be lower than the LBM which is a mass summation of internal organs/tissues excluding the adipose tissue (William *et al* 2006). There is no biologic upper limit of the body weight. Comparing the MRCPs with the phantoms with the 50th percentile standing height and body weight, there is not much difference for standing height (male: 0.5 cm and female: 0.3 cm), while there is large difference in body weight; that is, the body weight of the MRCPs is less than those of the 50th percentile phantoms by 6.3 kg and 4.1 kg for the male and female phantom, respectively. Note that, according to the ICRP, the reference values do not represent mean or median values (ICRP 1975, 2002).

Table 4 shows the anthropometric parameters (i.e., sitting height; head height, length, and breadth; sagittal abdominal diameter; and upper arm, waist, buttock, thigh, and calf circumferences) derived in the present study by multiple linear regressions of the anthropometric parameters for percentile-specific phantoms. The adjusted coefficient of determination (R^2) of the regressions were high, i.e., greater than 0.77, for most parameters except for head length and breadth, for which the R^2 values were less than 0.19. Note that the size of the head does not significantly change with standing height or body weight, and individual variability is dominant. It was at least confirmed that the head length and breadth are correlated to standing height and body weight considering that the calculated p-value is smaller than 0.1.

Table 3. 10th, 50th, and 90th percentile standing heights and body weights derived in present study for Caucasian adult population.

| Percentile | Male | | | Female | | |
|----------------------------------------|---------------------------------|---------------------------------|----------------------------------|---------------------------------|---------------------------------|---------------------------------|
| | Body weight 10 th | Body weight 50 th | Body weight 90 th | Body weight 10 th | Body weight 50 th | Body weight 90 th |
| Standing height 10 th | 167.2 cm 55.9 kg M_H10W10 | 167.2 cm 70.6 kg M_H10W50 | 167.2 cm 90.2 kg M_H10W90 | 154.9 cm 44.2 kg F_H10W10 | 154.9 cm 58.2 kg F_H10W50 | 154.9 cm 82.6 kg F_H10W90 |
| Standing height 50 th | 176.5 cm 64.7 kg M_H50W10 | 176.5 cm 79.3 kg M_H50W50 | 176.5 cm 99.1 kg M_H50W90 | 163.3 cm 49.9 kg F_H50W10 | 163.3 cm 64.1 kg F_H50W50 | 163.3 cm 88.4 kg F_H50W90 |
| Standing height 90 th | 185.8 cm 74.2 kg M_H90W10 | 185.8 cm 88.7 kg M_H90W50 | 185.8 cm 108.4 kg M_H90W90 | 171.7 cm 55.7 kg F_H90W10 | 171.7 cm 69.8 kg F_H90W50 | 171.7 cm 94.1 kg F_H90W90 |

Table 4. Anthropometric parameters derived in the present study.

| | Height percentile | Weight percentile | Sitting height [cm] | Head Height [cm] | Head length [cm] | Head breadth [cm] | Sagittal abdominal diameter [cm] | Upper arm circumference [cm] | Waist circumference [cm] | Buttock circumference [cm] | Thigh circumference [cm] | Calf circumference [cm] |
|--------|-------------------|-------------------|---------------------|------------------|------------------|-------------------|----------------------------------|------------------------------|--------------------------|----------------------------|--------------------------|-------------------------|
| Male | 10 th | 10 th | 88.5 | 22.8 | 19.3 | 15.0 | 17.3 | 28.7 | 77.2 | 85.9 | 46.2 | 33.9 |
| | | 50 th | 88.5 | 22.8 | 19.5 | 15.3 | 20.3 | 31.8 | 88.7 | 94.0 | 50.7 | 36.7 |
| | | 90 th | 88.5 | 22.8 | 19.8 | 15.6 | 24.2 | 35.9 | 104.0 | 104.8 | 56.9 | 40.4 |
| | 50 th | 10 th | 92.6 | 23.3 | 19.7 | 15.1 | 17.7 | 29.5 | 79.7 | 89.5 | 47.9 | 35.3 |
| | | 50 th | 92.6 | 23.3 | 19.9 | 15.3 | 20.7 | 32.6 | 91.1 | 97.6 | 52.5 | 38.0 |
| | | 90 th | 92.6 | 23.3 | 20.2 | 15.6 | 24.7 | 36.8 | 106.5 | 108.6 | 58.7 | 41.7 |
| | 90 th | 10 th | 96.6 | 23.8 | 20.0 | 15.2 | 18.3 | 30.5 | 82.7 | 93.6 | 49.9 | 36.7 |
| | | 50 th | 96.6 | 23.8 | 20.2 | 15.4 | 21.2 | 33.6 | 94.0 | 101.6 | 54.5 | 39.5 |
| | | 90 th | 96.6 | 23.8 | 20.5 | 15.7 | 25.2 | 37.7 | 109.4 | 112.5 | 60.6 | 43.2 |
| Female | 10 th | 10 th | 82.9 | 21.3 | 18.4 | 14.5 | 15.9 | 24.9 | 72.9 | 85.5 | 43.4 | 32.1 |
| | | 50 th | 82.9 | 21.3 | 18.6 | 14.6 | 18.8 | 28.5 | 83.7 | 95.4 | 48.6 | 35.0 |
| | | 90 th | 82.9 | 21.3 | 19.0 | 14.9 | 23.9 | 34.9 | 102.7 | 112.6 | 57.8 | 40.1 |
| | 50 th | 10 th | 86.6 | 21.7 | 18.7 | 14.6 | 15.7 | 25.1 | 73.9 | 87.8 | 44.6 | 33.2 |
| | | 50 th | 86.6 | 21.7 | 18.9 | 14.7 | 18.7 | 28.8 | 84.9 | 97.8 | 49.9 | 36.1 |
| | | 90 th | 86.6 | 21.7 | 19.3 | 15.0 | 23.8 | 35.1 | 103.7 | 114.9 | 59.1 | 41.2 |
| | 90 th | 10 th | 90.2 | 22.1 | 19.0 | 14.7 | 15.6 | 25.3 | 74.9 | 90.1 | 45.9 | 34.3 |
| | | 50 th | 90.2 | 22.1 | 19.3 | 14.8 | 18.6 | 29.0 | 85.9 | 100.1 | 51.2 | 37.2 |
| | | 90 th | 90.2 | 22.1 | 19.6 | 15.1 | 23.7 | 35.3 | 104.7 | 117.2 | 60.3 | 42.3 |

3.2. Constructed percentile-specific computational phantoms

Figure 3 shows the percentile-specific phantoms which were constructed to represent the adult male and female of 10th, 50th, and 90th percentiles in standing height and body weight. The constructed phantoms were exactly matched to the target values of standing height, body weight, head height, and sitting height, i.e., < 0.1% of difference. The phantoms also were matched to the target values of the other anthropometric parameters (i.e., upper arm, waist, buttock, thigh, and calf circumferences and sagittal abdominal diameter, listed in table 4) within 5% of difference. Tables 5 and 6 show the masses of the organs/tissues of the constructed phantoms for adult male and female, respectively, along with those of the MRCPs. Note that the masses of the most organs/tissues, except for the skin and breasts, were automatically determined during the scaling process. The masses of the skin and breasts were manually matched to the target values, the resulting differences being less than 0.1%.

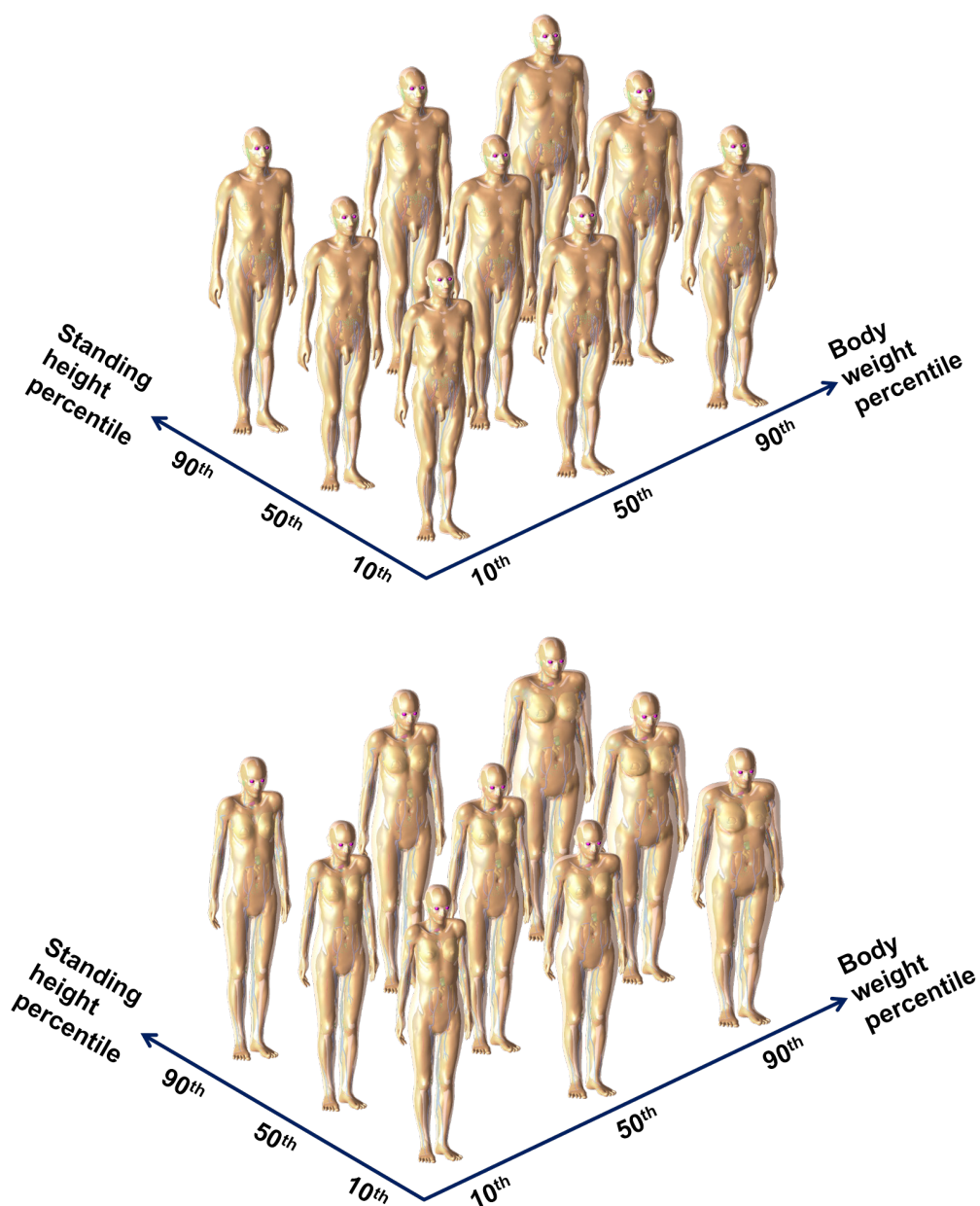


Figure 3. Constructed percentile-specific phantoms for male (upper) and female (lower).

Table 5. Organ/tissue masses of constructed phantoms and the MRCP for adult male. Note that the organ/tissue masses are inclusive of blood content.

(unit: grams)

| Organ/tissue | M_H10W10 | M_H10W50 | M_H10W90 | M_H50W10 | M_H50W50 | M_H50W90 | M_H90W10 | M_H90W50 | M_H90W90 | MRCP (male) |
|--------------------------|----------|----------|-----------|----------|-----------|-----------|-----------|-----------|-----------|----------------|
| Adrenals | 13.988 | 16.342 | 18.623 | 16.012 | 18.299 | 20.620 | 18.171 | 20.393 | 22.715 | 17.366 |
| ET | 35.914 | 39.178 | 42.487 | 38.744 | 41.864 | 45.181 | 41.723 | 44.717 | 47.995 | 40.874 |
| Oral mucosa | 0.114 | 0.127 | 0.140 | 0.123 | 0.136 | 0.148 | 0.134 | 0.145 | 0.158 | 0.132 |
| Trachea | 8.348 | 9.753 | 11.114 | 9.556 | 10.921 | 12.306 | 10.844 | 12.170 | 13.556 | 10.364 |
| BB ₁ | 2.557 | 2.987 | 3.403 | 2.926 | 3.344 | 3.769 | 3.321 | 3.727 | 4.151 | 3.173 |
| Arteries | 268.719 | 314.367 | 358.482 | 308.159 | 352.640 | 397.368 | 350.145 | 392.972 | 438.254 | 336.000 |
| Veins | 803.339 | 940.689 | 1076.133 | 259.292 | 1057.640 | 1192.713 | 1048.454 | 1177.205 | 1315.097 | 1008.000 |
| Skeletal system | 8135.244 | 9376.760 | 10585.302 | 9207.878 | 10412.774 | 11641.496 | 10349.606 | 11519.123 | 12746.623 | 9913.516 |
| Brain | 1431.537 | 1473.356 | 1523.986 | 1493.197 | 1534.699 | 1586.648 | 1557.758 | 1599.093 | 1651.645 | 1517.390 |
| Breasts, glandular | 8.345 | 9.750 | 11.110 | 9.553 | 10.917 | 12.302 | 10.841 | 12.166 | 13.552 | 10.360 |
| Breasts, adipose | 9.658 | 16.224 | 27.064 | 12.570 | 18.659 | 29.579 | 14.608 | 21.348 | 32.189 | 15.538 |
| Eye | 14.370 | 15.021 | 15.759 | 15.140 | 15.774 | 16.524 | 15.948 | 16.569 | 17.322 | 15.542 |
| Gallbladder wall | 8.348 | 9.753 | 11.114 | 9.556 | 10.921 | 12.306 | 10.844 | 12.170 | 13.556 | 10.364 |
| Gallbladder contents | 46.720 | 54.582 | 62.199 | 53.479 | 61.118 | 68.871 | 60.691 | 68.111 | 75.865 | 58.000 |
| Stomach wall | 156.490 | 182.823 | 208.334 | 179.128 | 204.714 | 230.684 | 203.283 | 228.136 | 254.111 | 194.271 |
| Stomach contents | 201.381 | 235.268 | 268.097 | 230.514 | 263.439 | 296.860 | 261.598 | 293.580 | 327.006 | 250.000 |
| Small Intestine wall | 694.846 | 811.769 | 925.042 | 795.365 | 908.970 | 1024.285 | 902.617 | 1012.969 | 1128.303 | 862.599 |
| Small Intestine contents | 281.934 | 329.375 | 375.336 | 322.719 | 368.815 | 415.603 | 366.237 | 411.012 | 457.809 | 350.000 |
| Colon wall | 397.157 | 463.968 | 528.731 | 454.611 | 519.544 | 585.456 | 515.854 | 578.988 | 644.748 | 493.040 |
| Colon contents | 241.657 | 282.322 | 321.716 | 276.617 | 316.127 | 356.232 | 313.917 | 352.296 | 392.408 | 300.000 |
| Heart wall | 310.803 | 363.102 | 413.769 | 355.765 | 406.580 | 458.160 | 403.738 | 453.098 | 504.687 | 385.839 |
| Blood in heart | 410.818 | 479.947 | 546.918 | 470.248 | 537.416 | 605.594 | 533.660 | 598.904 | 667.093 | 510.000 |
| Kidneys | 340.049 | 397.270 | 452.705 | 389.242 | 444.839 | 501.273 | 441.730 | 495.735 | 552.178 | 422.145 |
| Liver | 1901.039 | 2220.930 | 2530.836 | 2176.050 | 2486.865 | 2802.355 | 2469.483 | 2771.397 | 3086.941 | 2360.000 |
| Lungs | 965.614 | 1128.099 | 1285.513 | 1105.303 | 1263.178 | 1423.428 | 1254.349 | 1407.703 | 1567.981 | 1198.738 |
| Lymphatic nodes | 153.525 | 178.358 | 202.461 | 174.831 | 198.930 | 223.439 | 197.573 | 220.962 | 245.457 | 189.649 |

(Continued)

Table 6. Organ/tissue masses of constructed phantoms and the MRCP for adult female. Note that the organ/tissue masses are inclusive of blood content.

(unit: grams)

| Organ/tissue | F_H10W10 | F_H10W50 | F_H10W90 | F_H50W10 | F_H50W50 | F_H50W90 | F_H90W10 | F_H90W50 | F_H90W90 | MRCP (female) |
|--------------------------|----------|----------|----------|----------|----------|----------|----------|----------|----------|------------------|
| Adrenals | 12.246 | 14.625 | 17.044 | 13.761 | 16.169 | 18.739 | 15.316 | 17.718 | 20.459 | 15.466 |
| ET | 16.332 | 18.136 | 20.065 | 17.423 | 19.192 | 21.169 | 18.526 | 20.244 | 22.286 | 19.078 |
| Oral mucosa | 0.085 | 0.096 | 0.108 | 0.091 | 0.102 | 0.114 | 0.097 | 0.108 | 0.120 | 0.101 |
| Trachea | 6.494 | 7.753 | 9.035 | 7.287 | 8.560 | 9.920 | 8.100 | 9.369 | 10.818 | 8.201 |
| BB ₁ | 1.062 | 1.268 | 1.478 | 1.193 | 1.402 | 1.624 | 1.328 | 1.536 | 1.774 | 1.340 |
| Arteries | 193.419 | 230.947 | 269.078 | 217.513 | 255.476 | 296.005 | 242.258 | 280.244 | 323.423 | 246.000 |
| Veins | 580.088 | 692.892 | 807.413 | 652.581 | 766.624 | 888.367 | 726.938 | 840.819 | 970.794 | 737.998 |
| Skeletal system | 5908.205 | 6923.715 | 7964.369 | 6565.304 | 7591.569 | 8694.399 | 7238.446 | 8260.771 | 9434.210 | 7285.617 |
| Brain | 1274.300 | 1305.545 | 1351.932 | 1325.615 | 1357.412 | 1404.929 | 1378.142 | 1409.975 | 1458.881 | 1349.568 |
| Breasts, glandular | 162.317 | 193.842 | 225.915 | 182.399 | 214.314 | 248.382 | 203.009 | 234.847 | 271.180 | 204.982 |
| Breasts, adipose | 193.525 | 311.138 | 566.309 | 224.210 | 343.767 | 593.420 | 255.026 | 373.511 | 618.360 | 307.326 |
| Eye | 13.863 | 14.722 | 15.742 | 14.620 | 15.470 | 16.515 | 15.391 | 16.223 | 17.301 | 15.366 |
| Gallbladder wall | 6.494 | 7.755 | 9.039 | 7.298 | 8.574 | 9.937 | 8.122 | 9.396 | 10.850 | 8.201 |
| Gallbladder contents | 38.009 | 45.391 | 52.901 | 42.712 | 50.185 | 58.162 | 47.538 | 54.993 | 63.501 | 48.000 |
| Stomach wall | 136.891 | 163.477 | 190.526 | 153.827 | 180.742 | 209.473 | 171.208 | 198.059 | 228.700 | 172.873 |
| Stomach contents | 182.127 | 217.499 | 253.486 | 204.660 | 240.470 | 278.695 | 227.785 | 263.509 | 304.276 | 230.000 |
| Small Intestine wall | 598.461 | 714.691 | 832.942 | 672.502 | 790.171 | 915.763 | 748.482 | 865.870 | 999.834 | 757.768 |
| Small Intestine contents | 221.720 | 264.782 | 308.592 | 249.151 | 292.746 | 339.281 | 277.303 | 320.793 | 370.423 | 280.000 |
| Colon wall | 356.536 | 425.745 | 496.228 | 400.645 | 470.684 | 545.533 | 445.891 | 515.815 | 595.616 | 450.252 |
| Colon contents | 253.397 | 302.611 | 352.680 | 284.747 | 334.570 | 387.754 | 316.921 | 366.624 | 423.344 | 320.003 |
| Heart wall | 230.344 | 275.065 | 320.569 | 258.841 | 304.131 | 352.477 | 288.088 | 333.270 | 384.892 | 290.890 |
| Blood in heart | 292.988 | 349.890 | 407.782 | 329.236 | 386.843 | 448.336 | 366.436 | 423.905 | 489.487 | 370.000 |
| Kidneys | 282.618 | 337.507 | 393.350 | 317.583 | 373.151 | 432.468 | 353.467 | 408.902 | 472.163 | 356.905 |
| Liver | 1433.264 | 1711.625 | 1994.826 | 1610.585 | 1892.392 | 2193.210 | 1792.567 | 2073.699 | 2394.519 | 1810.000 |
| Lungs | 752.086 | 898.153 | 1046.758 | 845.133 | 993.007 | 1150.858 | 940.625 | 1088.146 | 1256.492 | 949.774 |
| Lymphatic nodes | 120.212 | 142.415 | 165.082 | 134.346 | 156.783 | 180.808 | 148.857 | 171.209 | 196.786 | 150.958 |

(Continued)

3.3. Organ-depth and chord-length distributions

Figure 4 shows the organ-depth distributions (ODDs) of selected organs (spongiosa, colon wall, and brains) measured from the front, back, left, right, top, and bottom body surfaces for M_H10W10, M_H50W50, M_H90W90, F_H10W10, F_H50W50, and F_H90W90 percentile-specific phantoms. For the ODD calculation, 10^7 points were randomly sampled in the considered organ/tissue, and the distances from the sampled points to the outer surface (i.e., front, back, left, right, top, and bottom body surfaces) of the phantoms were calculated. The ODDs represent the depth of an organ/tissue below the outer surface of the phantoms, influencing dose calculation for external exposure. It can be seen that the ODDs for the spongiosa and colon wall show a similar trend; that is, for a given organ, a larger phantom shows a broader distribution, and the distributions are noticeably different for different percentile phantoms. Our analysis of the results indicates that the ODDs faithfully reflect the scaling of the phantoms in the axial and transversal directions. For the brain, except for the bottom direction, the differences in the ODDs were much smaller for different percentile phantoms, which reflects the fact that the head dimensions do not significantly change as a function of standing height and body weight. Note that, from the 10th percentile to the 90th percentile phantoms, considering both the male and female phantoms, the head dimensions increase by only about 6-7%, while the other secondary anthropometric parameters increase by ~30%. For the bottom direction, the ODDs are significantly different even for the brain for different percentile phantoms, which reflects the differences in standing heights for different percentile phantoms.

Figures 5 shows the chord-length distributions (CLDs) for selected source regions (liver, lungs, and thyroid) and target regions (spongiosa, colon wall, lungs, stomach wall, breasts, and gonads) for M_H10W10, M_H50W50, M_H90W90, F_H10W10, F_H50W50, and F_H90W90 percentile-specific phantoms. For the CLD calculation, 10^7 point pairs were randomly sampled in the considered target and source regions, and distances of the point pairs were calculated. The CLDs represent a distance between the target and source regions, influencing dose calculation for internal exposure. Again, the CLDs well reflect the scaling of the phantoms in the axial and transversal directions, the broadening of the CLDs mainly depending on the sizes of the phantoms.

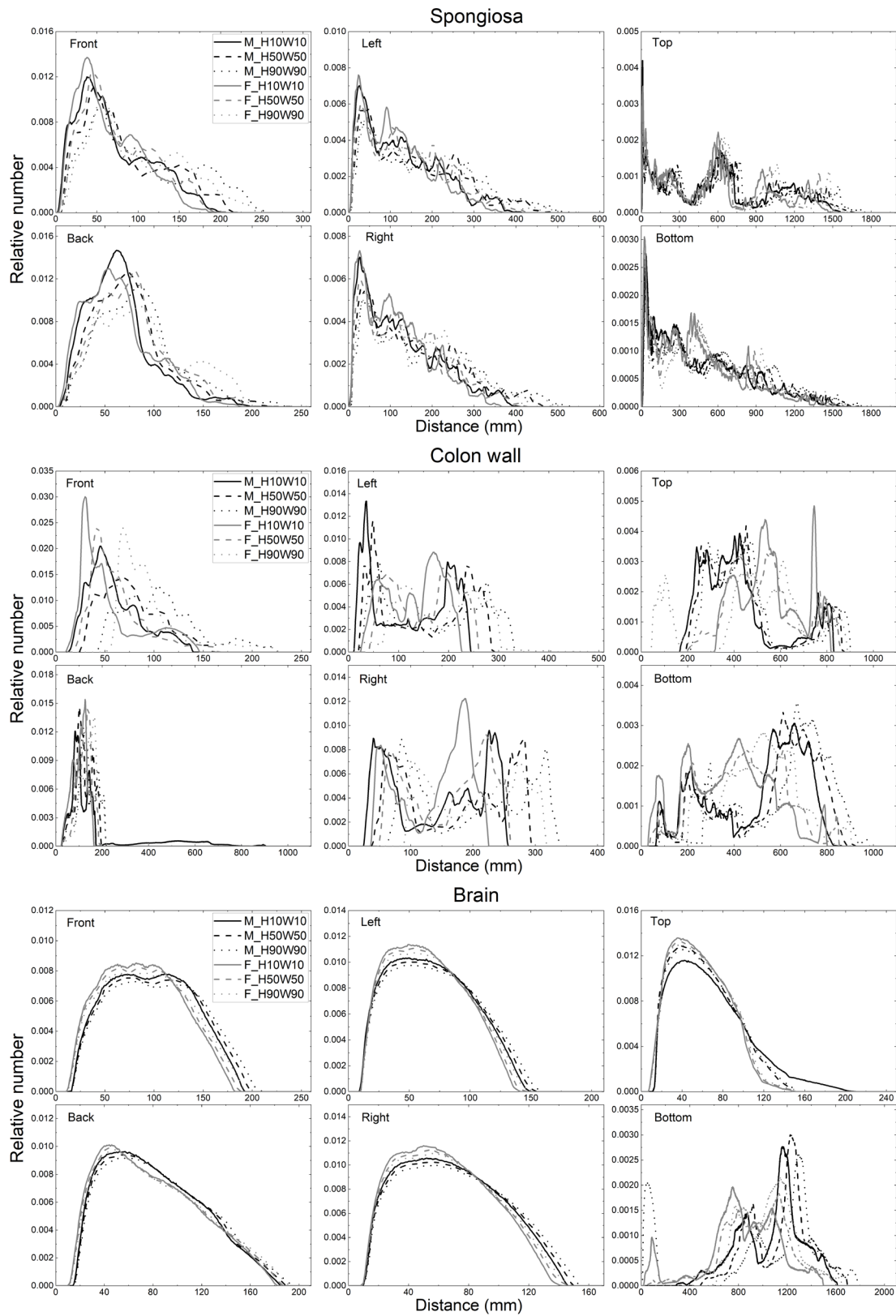


Figure 4. Organ-depth distributions (ODDs) - the distributions of depths of 10^7 randomly sampled points in selected organs (spongiosa, colon wall, and brains) below the body surfaces at: front, back, left, right, top, and bottom for M_H10W10, M_H50W50, M_H90W90, F_H10W10, F_H50W50, and F_H90W90 phantoms.

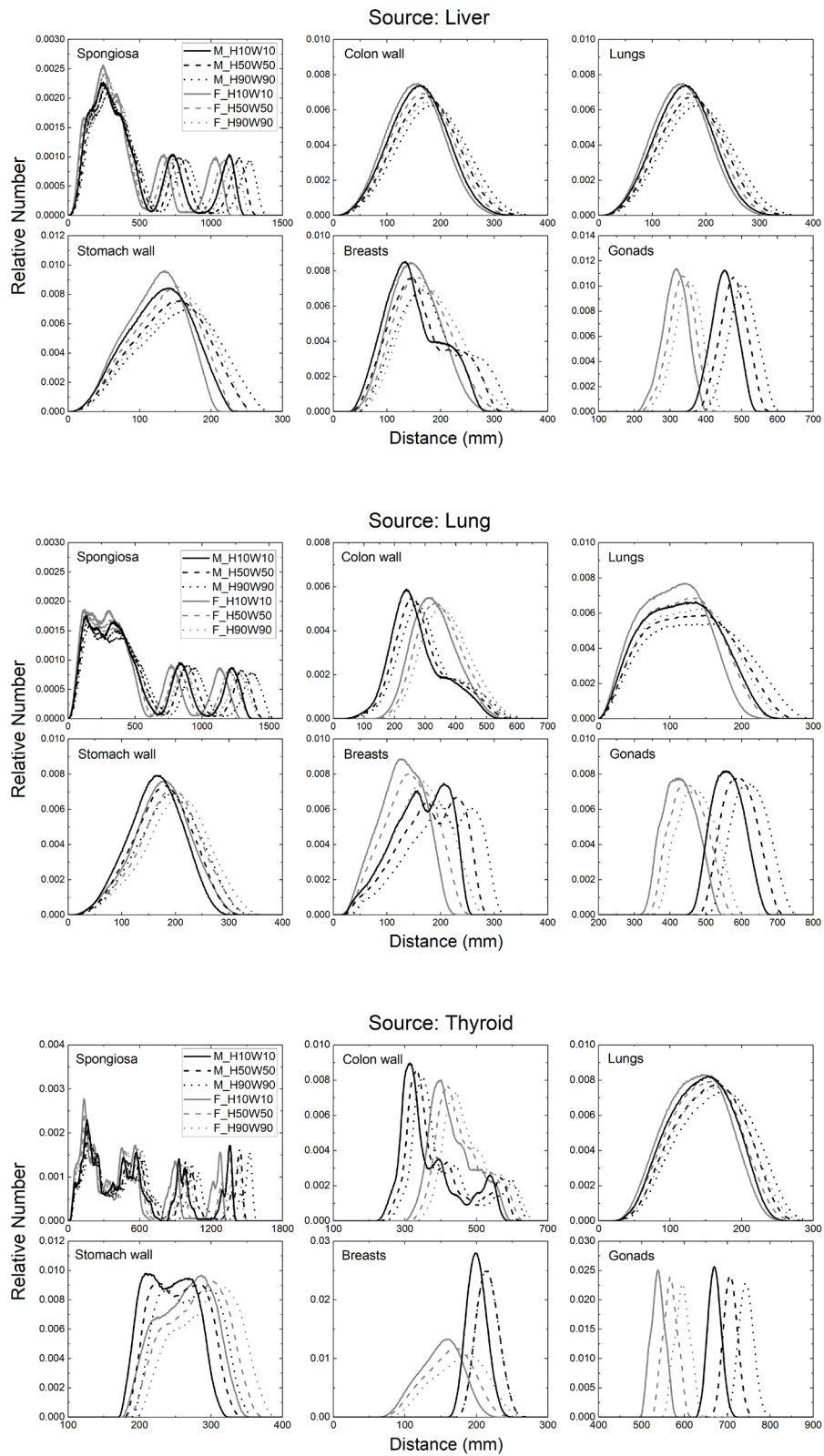


Figure 5. Chord-length distributions (CLDs) - the distributions of distances between 10^7 randomly sampled point pairs in selected source regions (liver, lungs, and thyroid) and target regions (spongiosa, colon wall, lungs, stomach wall, breasts, and gonads) for M_H10W10, M_H50W50, M_H90W90, F_H10W10, F_H50W50, and F_H90W90 phantoms.

3.4. Organ mass comparison with autopsy data

In the present study, the organ masses of the constructed phantoms were compared with the data of a French-based autopsy (Grandmaison *et al* 2001), in which 684 subjects were assembled into three groups, according to the body mass index (BMI) and the standing height, and then mean organ masses and their standard deviations were obtained for each group through forensic autopsy. Note that while organs of the phantoms were constructed considering the included blood contents, the organ masses of the autopsy data are generally between the masses *in vivo* (blood-inclusive) and parenchymal masses (blood-exclusive) because of the blood loss during the autopsy procedures. Lung mass of the autopsy data, however, is rather closer to the blood-inclusive mass, due to the autopsy techniques used by Grandmaison *et al* (2001) which presumed the lung mass inclusive of blood (ICRP 2002). For the consideration of the blood contents included in the organs, in the present study, blood-exclusive organ masses were additionally derived for analysis purpose, by subtracting blood content mass included in each organ calculated by the proportions of regional blood content of each organ of the MRCPs.

Figures 6 and 7 show the organ masses (blood-inclusive) of the constructed phantoms and the organ masses of the autopsy data, together with derived blood-exclusive organ masses, for the heart, kidneys, liver, lungs, pancreas, spleen and thyroid, according to the BMI and the standing height. For the heart, lungs, pancreas, spleen, and thyroid, the organ masses of the constructed phantoms tend to be larger than the autopsy values, but generally stay within one or two standard deviations from the mean of the autopsy data. On the other hand, the liver and kidney masses of the constructed phantoms show relatively large deviations from the autopsy data. These deviations can be explained by the fact that the organ masses of the MRCPs are the masses fully including regional blood content, unlike organ masses obtained by the autopsy. Note that, according to the data in ICRP Publication 89 (2002), the inclusion of regional blood content in the liver increases the liver mass by 31% and 29% for male and female, respectively, and the inclusion of the blood content in the kidneys increases the kidney mass by 36% and 30% for male and female. In addition, although the blood-inclusive organ masses are relatively larger than the autopsy data, the blood-exclusive organ masses of liver and kidney stay within one or two standard deviations from the mean of the autopsy data. Therefore, it can be generally concluded that the organ masses of the constructed phantoms are within reasonable ranges.

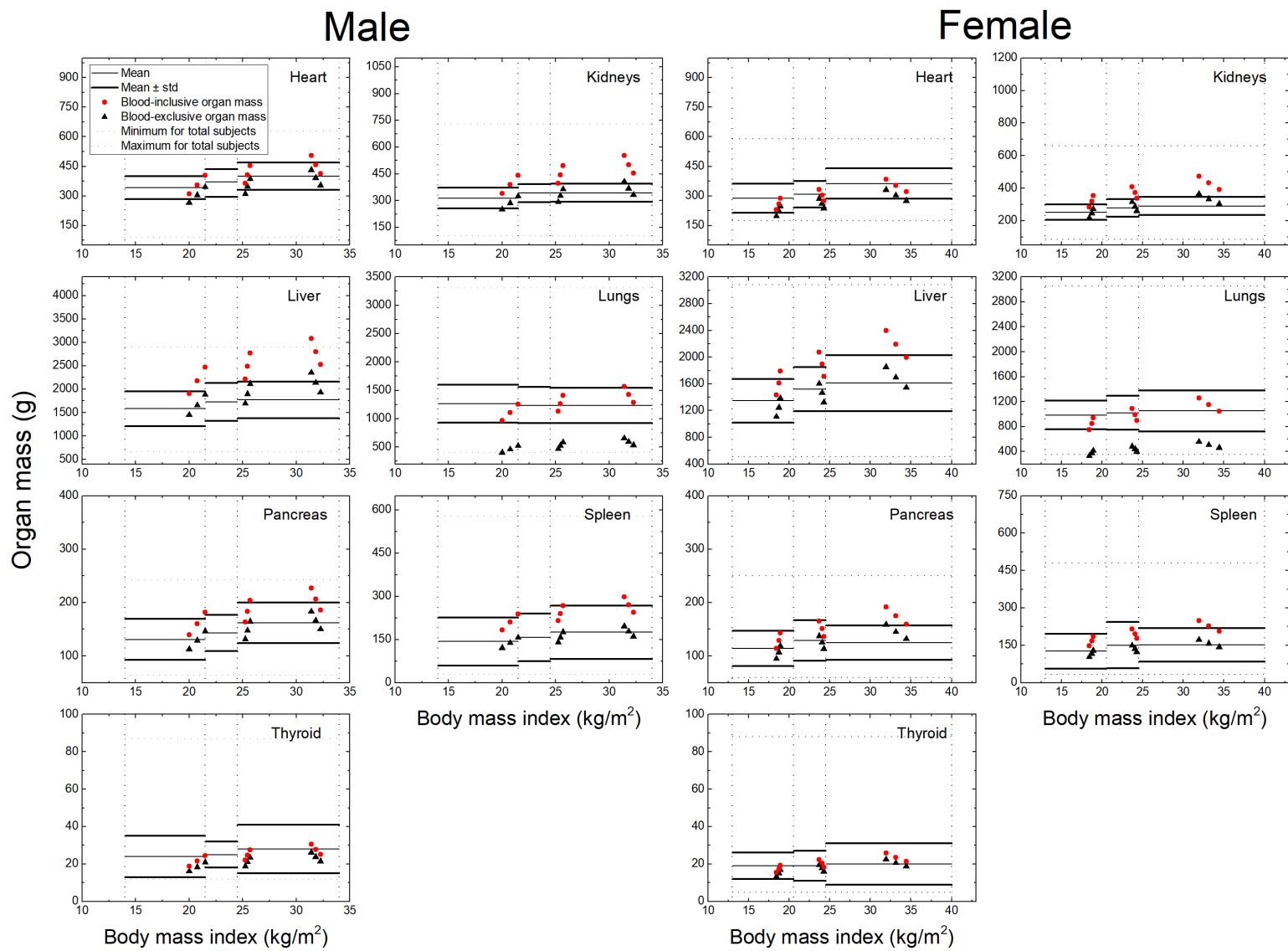


Figure 6. Comparison of organ masses of percentile-specific phantoms with autopsy data according to body mass index (BMI).

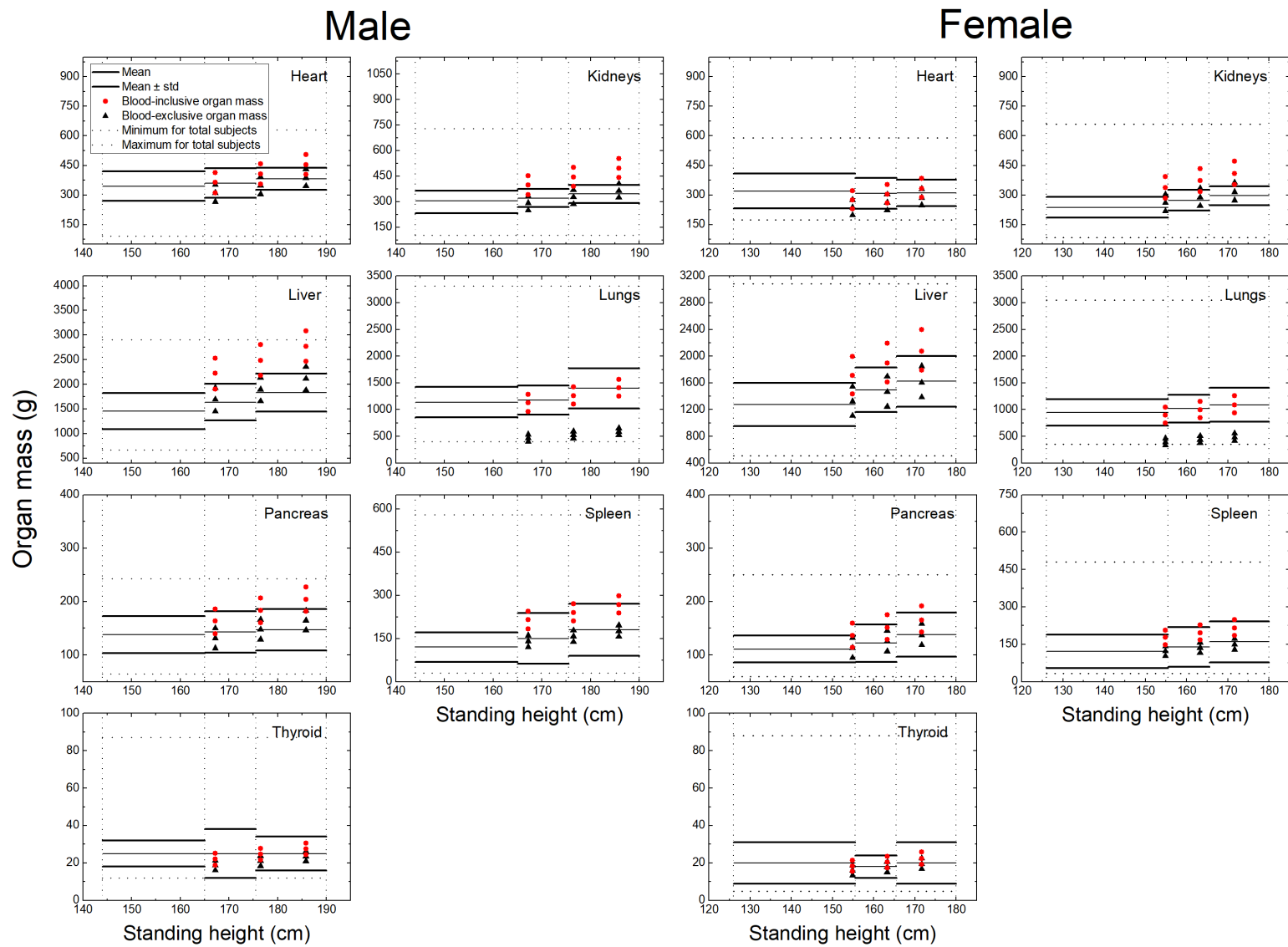


Figure 7. Comparison of organ masses of percentile-specific phantoms with autopsy data according to standing height.

3.5. Comparison of organ doses

The M_H10W10, M_H50W50, M_H90W90, F_H10W10, F_H50W50, and F_H90W90 percentile-specific phantoms were implemented in the Geant4 Monte Carlo code to calculate organ/tissue doses for exposures from a cesium-137 contaminated floor, and the calculated organ/tissue doses were compared with those of the MRCPs. Figure 8 shows the ratios of the organ absorbed dose of a percentile-specific phantom and that of the MRCP for selected organs.

The results showed that organ absorbed doses of the 50th percentile phantoms (i.e., M_H50M50 and F_H50M50) are indeed very close to those of the MRCPs, generally differences being less than 10%. In particular, the organs/tissues with relatively large tissue weighting factor ($w_T \geq 0.08$) (i.e., RBM, colon, lungs, stomach, breasts, and gonads) show minimal differences, i.e., less than 5%. Therefore, although the body weight of the MRCPs is less than those of the 50th percentile phantoms by 6.3 kg and 4.1 kg for the male and female phantom, respectively, it can be concluded that, for at least this case, the MRCPs properly represent the Caucasian population for radiation protection purpose.

On the other hand, there were noticeable differences of the organ absorbed doses for the 10th and 90th percentile phantoms when compared to the MRCPs. The 10th percentile phantom receives higher doses for all organs/tissues than the MRCPs, with maximum differences of 26% and 23% (in thyroid dose) for the male and female phantom, respectively. On the contrary, the 90th percentile phantom receives lower doses than the MRCPs, with maximum differences of 30% and 38% (in thyroid dose) for the male and female phantom, respectively. These results confirm the general intuition that a small person receives higher doses than a large person when exposed to a static radiation field; and organs closer to the source receive higher absorbed doses.

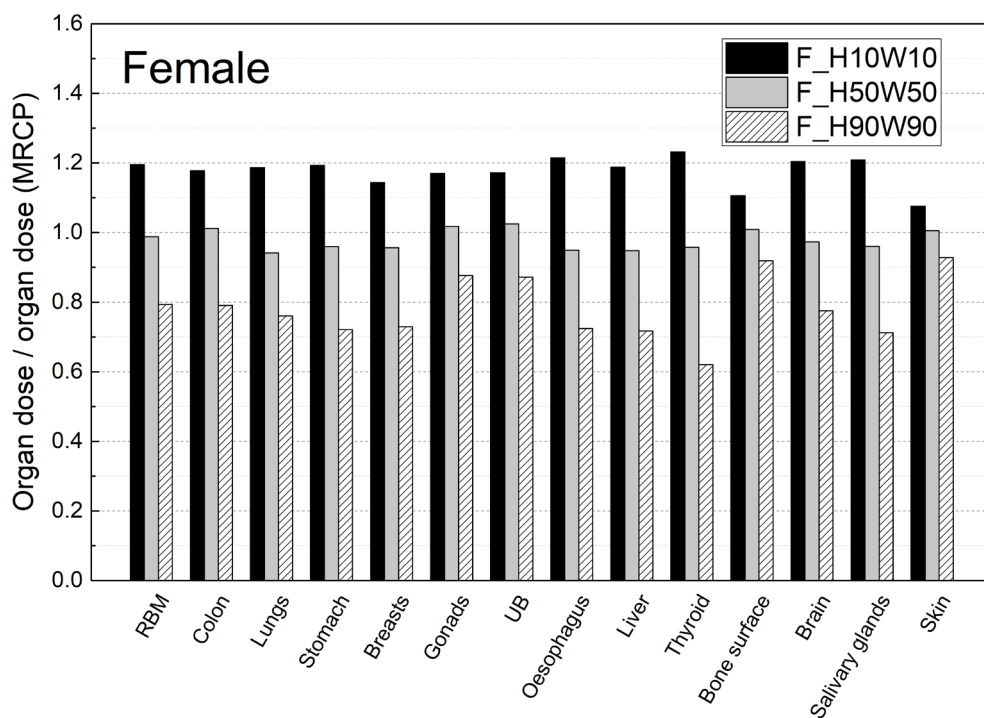
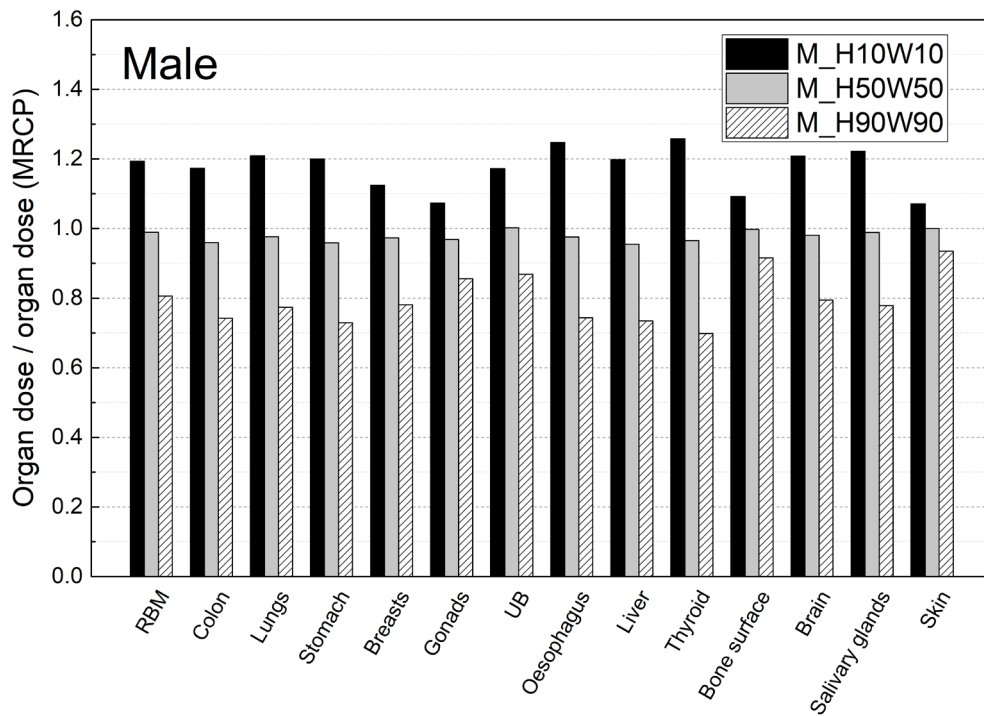


Figure 8. Comparison of organ doses (= organ or tissue-averaged absorbed doses) of H10W10, H50W50, and H90W90 percentile-specific phantoms with those of the MRCPs for male (upper) and female (lower) for gamma irradiation by cesium-137 contamination on floor. Bar graph shows ratios of organ dose of percentile-specific phantom to organ dose of the MRCP for selected organs and tissues.

4. Conclusion

In the present study, the adult MRCPs were deformed to produce a set of percentile-specific adult phantoms which represent 10th, 50th, and 90th percentile standing heights and body weights in adult male female Caucasian populations. For this phantom construction, the anthropometric parameters were first derived for the percentile-specific phantoms, and the MRCPs were matched to the parameters to produce percentile-specific phantoms. Then, the effect and validity of scaling and adjustments were investigated by calculating organ depth and cord length distributions and by comparing the organ masses with available autopsy data. The constructed phantoms were also used to calculate organ doses for a cesium-137 contaminated floor, and the calculated values were compared with those of the MRCPs. The results of dose calculations showed that the organ doses of the 50th percentile (i.e., M_H50M50 and F_H50M50) phantoms are close to those of the MRCPs. However, there were noticeable differences of the organ doses for the 10th and 90th percentile phantoms when compared to the MRCPs, confirming the general intuition that a small person receives higher doses than a large person when exposed to a static radiation field; and organs closer to the source receive higher absorbed doses. In the near future, the methodology developed in the present study will be automated to produce a phantom library with various body sizes, for which manual deformation is not acceptable considering the number of phantoms to be produced.

Acknowledgments

The authors thank Hyojoo Kim, Jong Chan Jung, Sang Hyun Jun and Jeong Yeol Baek, in the Department of Nuclear Engineering at Hanyang University in Seoul, Korea, for their time and efforts to construct percentile-specific phantoms. This work was supported by Nuclear Safety Research Development (NSR&D) Program through Korea Foundation of Nuclear Safety (KoFONS), funded by the Nuclear Safety and Security Commission (NSSC), and additionally, by the National Research Foundation of Korea (NRF) funded by the Ministry of Science, ICT and Future Planning through the National Research Foundation of Korea (Project No.: 1705006, 2016R1D1A1A09916337). Two of the authors (Chansoo Choi and Haegin Han) were supported by the Global PhD Fellowship program (Project No.: NRF-2017H1A2A1046391, NRF-2018H1A2A1059767), and one of the authors (Yeon Soo Yeom) was supported by a grant of the Korean Health Technology R&D Project through the Korean Health Industry Development Institute (KHIDI), funded by the Ministry of Health & Welfare, Republic of Korea (Project No: H18C2257).

References

- Akhavanallaf A, Xie T and Zaidi H 2018 Development of a library of adult computational phantoms based on anthropometric indexes *IEEE. Trans. Radiat. Plasma. Med. Sci.* Online: <https://doi.org/10.1109/TRPMS.2018.2816072>
- Allison J, Amako K, Apostolakis J, Arce P, Asai M, Aso T, Bagli E, Bagulya A, Banerjee S and Barrand G 2016 Recent developments in Geant4 Nucl. Instrum. Methods Phys. Res. A **835** 186–225
- Bochud F O, Laedermann J P, Baechler S, Bailat C J, Boschung M, Aroua A and Mayer S 2014 Monte Carlo simulation of a whole-body counter using IGOR phantoms *Radiat. Prot. Dosim.* **162** 280–8
- Boer P 1984 Estimated lean body mass as an index for normalization of body fluid volumes in humans *Am. J. Physiol. Renal Physiol.* **247** 632–6
- Bosy-Westphal A, Reinecke U, Schloerke T, Illner K, Kutzner D, Heller M and Müller M J 2004

- Effect of organ and tissue masses on resting energy expenditure in underweight, normal weight and obese adults *Int. J. Obes.* **28** 72–9
- Cassola V F, Milian F M, Kramer R, de Oliveira Lira C A B and Khoury H J 2011 Standing adult human phantoms based on 10th, 50th and 90th mass and height percentiles of male and female Caucasian populations *Phys. Med. Biol.* **56** 3749–72
- Chen Y, Qiu R, Li C, Wu Z and Li J 2016 Construction of Chinese adult male phantom library and its application in the virtual calibration of in vivo measurement *Phys. Med. Biol.* **61** 2124–44
- Clairand I, Huet C, Trompier F and Bottollier-Depois J F 2008 Physical dosimetric reconstruction of a radiological accident due to gammagraphy equipment that occurred in Dakar and Abidjan in summer 2006 *Radiat. Meas.* **43** 698–703
- Courageot E, Huet C, Clairand I, Bottollier-Depois J F and Gourmelon P 2010 Numerical dosimetric reconstruction of a radiological accident in South America in April 2009 *Radiat. Prot. Dosim.* **144** 540–2
- de la Grandmaison G L, Clairand I, and Durigon M, 2001 Organ weight in 684 adult autopsies: new tables for a Caucasoid population *Forensic Sci. Int.* **119** 149–54
- Deurenberg P, Weststrate J A and Seidell J C 1991 Body mass index as a measure of body fatness: age- and sex-specific prediction formulas *Br. J. Nutr.* **65** 105–14
- Ding A, Mille M M, Liu T, Caracappa P F and Xu X G 2012 Extension of RPI-adult male and female computational phantoms to obese patients and a Monte Carlo study on the effects on CT imaging dose *Phys. Med. Biol.* **57** 2441–59
- Eakins J S and Kouroukla E 2015 Luminescence-based retrospective dosimetry using Al₂O₃ from mobile phones: a simulation approach to determine the effects of position *J. Radiol. Prot.* **35** 343–81
- Geyer A M, O'Reilly S, Lee C, Long D J and Bolch W E 2014 The UF/NCI family of hybrid computational phantoms representing the current US population of male and female children and adolescents—applications to CT dosimetry *Phys. Med. Biol.* **59** 5225–42
- Gordon C C, Blackwell C L, Bradtmiller B, Parham J L, Barrientos P, Paquette S P, Corner B D, Carson J M, Venezia J C, Rockwell B M, Mucher M and Kristensen S 2014 2012 Anthropometric survey of U.S. army personnel: methods and summary statistics (NATICK/TR-15/007) U.S. Army Natick Soldier Research, Development and Engineering Center, Natick, Massachusetts
- Hume R 1966 Prediction of lean body mass from height and weight *J. Clin. Pathol.* **19** 389–91
- ICRP 1975 Report of the Task Group on Reference Man (Annals ICRP (ICRP Publication 23) vol 4) (Oxford: Pergamon)
- ICRP 2002 Basic Anatomical and Physiological Data for Use in Radiological Protection: Reference Values (Annals ICRP (ICRP Publication 89) vol 32) (Oxford: Pergamon)
- ICRP 2008 Nuclear Decay Data for Dosimetric Calculations (Annals ICRP (ICRP Publication 107) vol 38) (Amsterdam: Elsevier)
- ICRP 2009 Adult Reference Computational Phantoms (ICRP Publication 110) (Oxford: Pergamon)
- ICRP 2010 Conversion Coefficients for Radiological Protection Quantities for External Radiation Exposures (Annals ICRP (ICRP Publication 116) vol 40) (Amsterdam: Elsevier)
- James W P T and Waterlow J C 1976 Research on obesity: a report of the DHSS/MRC group HM Stationery Office
- Johnson P B, Whalen S R, Wayson M, Juneja B, Lee C and Bolch W E 2009 Hybrid patient-dependent phantoms covering statistical distributions of body morphometry in the US adult and pediatric population *Proc. IEEE* **97** 2060–75
- Kim C H et al 2018 New mesh-type phantoms and their dosimetric applications, including emergencies *Ann. ICRP Online*: <https://doi.org/10.1177/0146645318756231>
- Lu W, Wu Z, Qiu R, Li C, Yang B, Gao S, Ren L and Li J 2017 Physical dosimetric reconstruction of a radiological accident at Nanjing (China) for clinical treatment using Thudose *Health. Phys.* **113** 327–34
- McArdle W D, Katch F I and Katch V L 2006 *Essentials of Exercise Physiology* Lippincott Williams & Wilkins
- Na Y H, Zhang B, Zhang J, Caracappa P F and Xu X G 2010 Deformable adult human phantoms for

- radiation protection dosimetry: anthropometric data representing size distributions of adult worker populations and software algorithms *Phys. Med. Biol.* **55** 3789–811
- Pierrat N, de Carlan L, Cavadore D and Franck D 2005 Application of Monte Carlo calculation for the virtual calibration of a low-energy in vivo counting system IEEE. *Trans. Nucl. Sci.* **52** 1353–8
- Pieterman R, Willemsen A, Appel M, Pruim J and Koëter G 2002 Visualisation and assessment of the protein synthesis rate of lung cancer using carbon-11 tyrosine and positron emission tomography *Eur. J. Nucl. Med. Mol. Imaging* **29** 243–47
- Qiu R, Li J, Zhang Z, Wu Z, Zeng Z and Fan J 2008 Photon SAF calculation based on the Chinese mathematical phantom and comparison with the ORNL phantoms *Health Phys.* **95** 716–24
- Si H 2006 A quality tetrahedral mesh generator and three-dimensional delaunay triangulator version 1.4 User's Manual Online: <http://tetgen.berlios.de/index.html>
- United Nations, Department of Economic and Social Affairs, Population division 2017 world population prospects: the 2017 revision, DVD edition
- Yeom Y S, Jeong J H, Han M C and Kim C H 2014 Tetrahedral-mesh-based computational human phantom for fast Monte Carlo dose calculations *Phys. Med. Biol.* **59** 3173–85